JOURNAL OF GEOPHYSICAL RESEARCH, VOL. 85, NO. B7, PAGES 3751-3758, JULY 10, 1980

A Compensation Mechanism for the Central Pacific

D. T. SANDWELL AND K. A. POEHLS[1]

Department of Earth and Space Sciences, University of California, Los Angeles, California 90024

Geos 3 derived geoid heights and sea floor topography were averaged into 256 square areas (203 km on a side) for a region in the central Pacific containing a large portion of the Hawaiian Island chain. The whole region is about 500 m shallower than normal sea floor of the same age. The major portion of the depth anomaly is the Hawaiian swell. Data were analyzed using a two-dimensional fast Fourier transform. A transfer function was computed to determine the part of the observed geoid height that is coherent and in phase with the topography. A number of compensation models were tested against this function. Of these models no single physically reasonable model was found to have an acceptable fit. Accordingly, two models were introduced, one compensating short-wavelength topography at a shallow depth (14 km) and the other compensating the longer wavelengths by a deep mechanism. Acceptable deep compensation models include Airy-Heiskanen type compensation at depths between 40 and 80 km. Using the transition wavelength between the two models (1100 km), an estimate is made of the amplitude and shape of the heat anomaly needed to uplift the Hawaiian swell. The peak of the anomaly has an amplitude of 530 mW m^{-2} and is located 275 km east of Hawaii.

INTRODUCTION

The Hawaiian ridge appears to be a midplate feature that is not related to the sea floor spreading process. The topography, surrounding the volcanic islands, is characterized by a broad swell of 1000 to 2000-km width upon which are superimposed several rises and deeps. The deeps and rises have been explained as the flexural response of the lithosphere to loading by the island chain [*Walcott*, 1970]. The origin of the Hawaiian swell has not yet been adequately explained.

Numerous origins for the Hawaiian swell and Hawaiian-Emperor seamount chain have appeared in the literature. These include propagating lithospheric cracks [*McDougall*, 1971], deep mantle plumes [*Wilson*, 1963], shallow mantle plumes or heating anomalies [*Shaw and Jackson*, 1973; *Shaw*, 1973] and asthenospheric bumps [*Menard*, 1973]. The most popular of these hypotheses are those dealing with the thermal anomalies. Recently, *Detrick and Crough* [1978] presented evidence showing that gouyots along the Hawaiian-Emperor chain have subsided at a rate higher than the rate predicted by the empirical depth-age relation. They invoked a lithospheric thinning mechanism to explain both the Hawaiian swell and the increased subsidence rate of gouyots along the swell. This idea is, of course, consistent with the presence of a thermal anomaly.

In this study we analyze a region in the central Pacific containing a large portion of the Hawaiian chain. Our aim is to determine an average compensation mechanism for the sea floor topography at wavelengths between 300 and 3000 km. To accomplish this, a transfer function between geoid height and topography is computed. A number of compensation models are tested, and an acceptable class of models is found. An acceptable model must meet the following criteria: the model must fit the data, it must be physically reasonable, and it should be consistent with other geophysical observations.

When working with geoid or gravity data, many compensation models can be found that fit within the uncertainties in the data. Because of this, the class of models must be narrowed by requiring that they be physically reasonable. We test the simplest models first and either accept or reject them before moving on to more complex models. By using this method the unacceptable aspects of the rejected models are clearly pointed out.

The current compensation models for the central Pacific are divided into two classes. Investigators who have looked at the relationship between gravity and topography at the longer wavelengths (>1000 km) have found that compensation occurs at depths between 50 and 120 km [*Watts*, 1976; *Detrick and Crough*, 1978; *Crough*, 1978]. *Watts* [1978] has shown that the shorter wavelength topography (<600 km), across the Hawaiian Emperor island chain, is supported by the strength of the lithosphere. Upon closer inspection, it is clear that neither model fits the data over the whole wavelength spectrum.

The data presented here cover both of these wavelength regimes. We show that there is no single, physically reasonable, compensation mechanism that fits the data at all wavelengths. We then introduce a more complex model with two competing compensation mechanisms, one dominating at shorter wavelengths and the other at longer wavelengths. Using these results, we reconsider the lithospheric thinning hypothesis. By modeling the lithosphere as a thermal boundary layer an estimate is made for the heat flow necessary to uplift the Hawaiian swell. A major purpose of this study is to demonstrate why two compensation mechanisms are necessary and to determine at what wavelength the transition occurs.

DATA

The area investigated in this study is outlined in Figure 1. The main tectonic features included in this region are the Musician seamounts, the Hawaiian island chain, the Hawaiian swell, the Necker ridge, the eastern part of the mid-Pacific mountains, the northern end of the Line islands, and a number of fracture zones. For the analysis technique used below, it was assumed that all of these major topographic features have the same wavelength-dependent compensation mechanism. To focus upon the compensation mechanism for the Hawaiian swell, the size of the region was chosen small enough so that the swell was the dominant tectonic feature at the longer wavelengths and large enough so that the topography power spectrum reached its peak at a wavelength shorter than the side length of the region. For analysis purposes the

[1] Now at Dynamics Technology, Inc., Torrance, California 90503.

Paper number 80B0310.
0148-0227/80/080B-0310$01.00

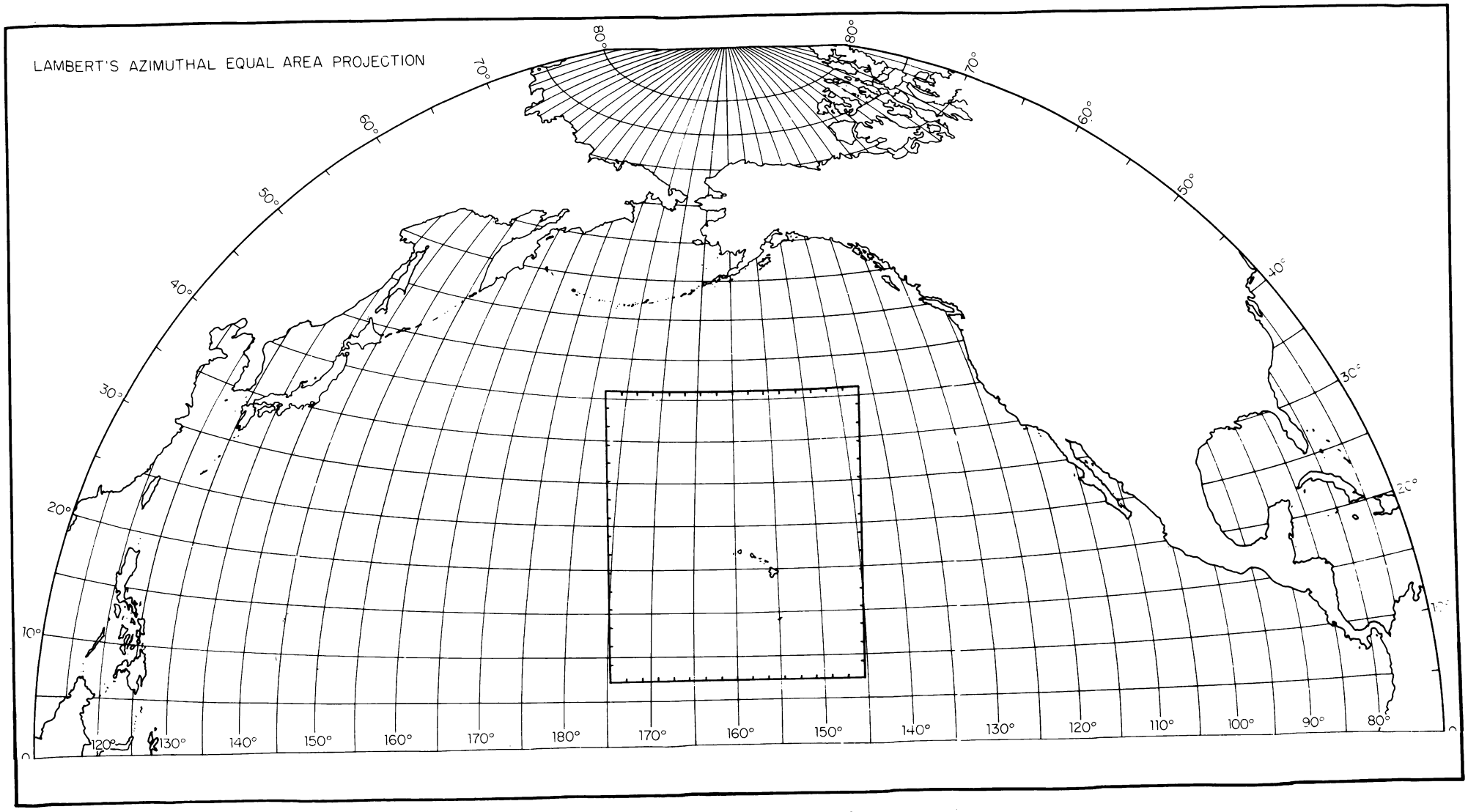

Fig. 1. Location map and outline of study area.

area was divided into 256 equal area squares with side length of 203 km (approximately 2° × 2°). Geoid height and sea floor depth estimates for each square were obtained by graphically integrating over the area. A mean and best fitting plane were removed from each data set before a two-square taper was added to the perimeter.

Bathymetry. Sea floor bathymetry was taken from *Chase et al.* [1970] and was corrected for water velocity using Matthews tables [*Matthews*, 1939]. No sediment corrections were applied to the data because the sedimentary cover is regionally uniform [*Ewing et al.*, 1968] and the large averaging areas largely negate the influences of local accumulations. Figure 2 shows the results after averaging. The WNW striking island chain can clearly be seen. The deep and rise flanking the island chain do not show up after averaging becuase the box size is greater than the wavelength of these features. The Hawaiian swell shows up clearly with a strike similar to the island chain and a half width of about 1000 km. The swell is elongate on the north but drops sharply to the south at the southeast end of the chain. The mean depth of the region (5169 m) fits the empirical depth-age curve at about 60 m.y.; the magnetic age of the area is closer to 100 m.y.

Geoid. Sea surface heights measured by the Geos 3 altimeter were used in this study. The numerous individual satellite passes were processed in a way that minimized both orbital tracking errors and track crossing discrepancies [*Brace*, 1977]. The data were averaged into the same squares as the bathymetry (Figure 3). The dominant feature in the geoid is the long-wavelength high over the Hawaiian swell region with an amplitude of roughly 10 m. The central portion of this high has a feature elongated in the WNW direction. This feature probably reflects the part of the geoid produced by the island chain. The remainder of the high is roughly circular with a half width of about 1200 km in the N-S direction and about 1600 km in the E-W direction. The peak-to-trough amplitude in the E-W direction is about 12 m, and in the N-S direction it is only 10 m.

Geoid data were used in this analysis for a number of reasons. First, these data are best suited for studies at intermediate wavelengths. At the shorter wavelengths, geoid undulations have a low signal-to-noise ratio. At the longer wavelengths (degree <10) the Geos 3 derived geoid may contain inaccuracies due to satellite tracking errors. The second reason these data were used is because *Watts* [1976] has used surface gravity data to infer the lithospheric and upper mantle density structure over a region roughly the same as that shown in Figure 1. Since the Geos 3 geoid and the surface gravity measurements are independent data sets, it is interesting to compare the results of the two anlayses.

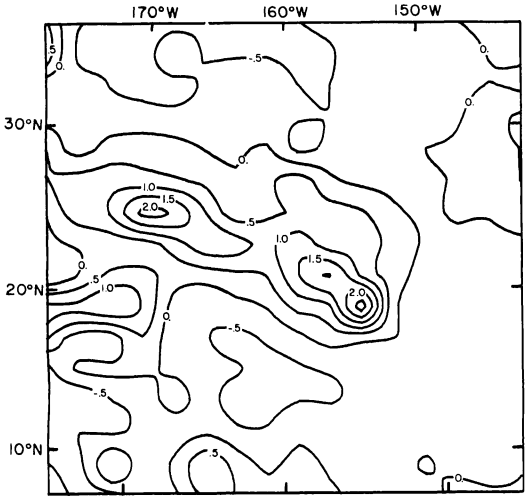

Fig. 2. Sea floor topography averaged into areas 203 km on a side with best-fitting plane removed. Map was made by contouring the digitized data. Contour units are in kilometers.

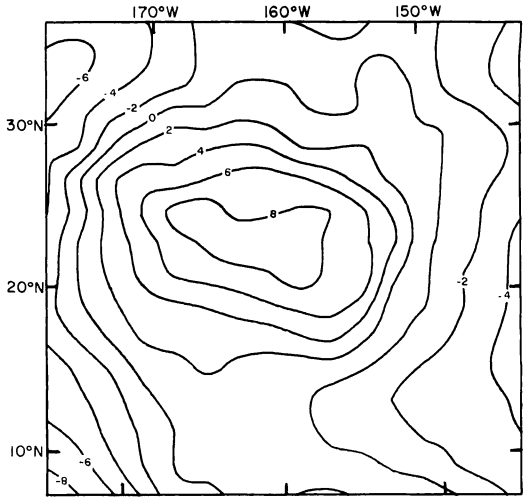

Fig. 3. Geoid heights (in meters) averaged into areas 203 km on a side with best fitting plane removed.

Estimation of the Transfer Function

The transfer function is used to separate the observed geoid into two parts. Following the approach of *Dorman and Lewis* [1970], we write

$$N(\mathbf{k}) = Q(k)T(\mathbf{k}) + I(\mathbf{k}) \tag{1}$$

$N(\mathbf{k})$ is the two-dimensional Fourier transform of the geoid, and the quantity $Q(k)T(\mathbf{k})$ is the part of the geoid that is linearly related to the Fourier transform of the topography $T(\mathbf{k})$. $I(\mathbf{k})$ does not correlate, on the average, with the topography. By minimizing the sum of $I(\mathbf{k})$ squared, the best estimate of the transfer function is

$$Q(k) = \mathrm{Re}\left[\frac{\langle NT^* \rangle}{\langle TT^* \rangle}\right] \tag{2}$$

The angle brackets denote averaging over an annulus in the wave number domain. In writing (2) it is assumed that the transfer function is linear, real, and isotropic. An estimate for the uncertainty in the transfer function is [*McNutt*, 1978]

$$\sigma^2(k) = \frac{1}{(2n-1)}\left[\frac{\langle GG^* \rangle}{\langle TT^* \rangle} - Q^2\right] \tag{3}$$

where n is the number of complex numbers within the averaging interval.

The Fourier transform of both the geoid and topography must be known in order to calculate the transfer function. To satisfy the sampling theorem, the short wavelengths were removed from each data set by averaging over equal area squares. The center of each box was assigned this average value. This averaging procedure introduces errors in the Fourier transform at short wavelengths but has a negligible effect upon the longer-wavelength part of the transform. Because of

TABLE 1. Estimates of the Transfer Function

Wavelength λ, km	Transfer Function Q, m/m $\times 10^{-3}$	Phase ϕ	Coherence γ^2	Uncertainty σ, m/m $\times 10^{-3}$	Transfer Function Q,[1] mgal/km	Uncertainty σ, mgal/km	Power Topography TT^*, m$^2 \times 10^4$	Power Geoid NN^*, m^2
3617	8.77	−6.1	0.270	7.28	14.9	12.4	1.72	5.98
2678	7.75	24.3	0.759	2.76	17.8	6.3	1.29	1.23
1860	4.93	−1.3	0.534	1.27	16.3	4.2	4.57	2.09
1314	3.54	11.3	0.309	1.08	16.6	5.0	3.52	1.48
935	0.25	69.9	0.011	1.02	1.7	6.6	1.36	0.66
669	0.82	−15.4	0.143	0.22	7.5	2.1	1.37	0.07
479	0.57	19.4	0.078	0.16	7.4	2.1	1.53	0.07
344	0.21	35.2	0.028	0.15	9.3	2.7	0.75	0.002

[1]The transfer function was converted from meters per meter to milligals per kilometer by multiplying by $2\pi\bar{g}/\lambda$.

this averaging scheme the two shortest-wavelength estimates may be biased. A better method of removing the short wavelengths before taking the discrete Fourier transform is to use a smoother low-pass filter such as a Gaussian filter.

The results of the transfer function analysis are given in Table 1. About 40% of the power in the geoid is coherent and in phase with the topography. This part is shown in Figure 4. To facilitate comparison with past work, the transfer function was converted to a free air anomaly transfer function (Table 1) and a Bouguer anomaly transfer function (using density ρ_0 of 1800 kg m^{-3}, Figure 5). If the region is isostatically compensated then the transfer function (Figure 5) approaches $-2\pi G\rho_0$ as the wavelength goes to infinity and approaches zero as the wavelength goes to zero. The shape of the transfer function between these two extremes contains information about the compensation mechanism [*Dorman and Lewis*, 1972]. Figure 5 shows that the transfer function for the central Pacific makes an abrupt jump at a wavelength of about 1100 km.

Compensation Models

It is well known that given the geoid height over the surface of the earth, the density anomalies causing the geoid undulations cannot be uniquely determined. This fact is clearly seen in the following equation, where the spherical harmonic coefficients of the geoid N_{lm} are related to the coefficients of the density anomaly $\Delta\rho_{lm}(r)$:

$$N_{lm} = \frac{4\pi R^4}{M(2l+1)} \int_0^1 \mu^{l+2} \Delta\rho_{lm}(\mu R)\, d\mu \tag{4}$$

R is the radius of the earth, $\mu = r/R$ is the normalized radius, and M is the mass of the earth. Before (4) can be inverted, certain simplifying assumptions must be made about the earth. *Lewis and Dorman* [1970] observed that the relationship between Bouguer anomaly and topography in the wave number domain was nearly linear and isotropic. These observations led them to decompose the compensating density in the following way:

$$\Delta\rho_{lm}(r) = \rho(r, l) T_{lm} \tag{5}$$

Inserting (5) into (4) and dividing by the spherical harmonic coefficients of the topography T_{lm}, we obtain

$$Q_l = \frac{4\pi R^4}{M(2l+1)} \int_0^1 \mu^{l+2} \rho(\mu R, l)\, d\mu \tag{6}$$

where Q_l is the transfer function and $\rho(\mu R, l)$ is a Green function relating a point topographic load to its compensating density at some depth and degree. All local and regional compensation models can be represented by this Green function. These models include Pratt, Airy (to a linear approximation), and elastic plate models. For $l = 0$, equation (6) is just a statement of mass conservation. Notice that the function $\rho(\mu R, l)$ is not a density but has units of mass per length to the fourth power and is a density per unit of topography.

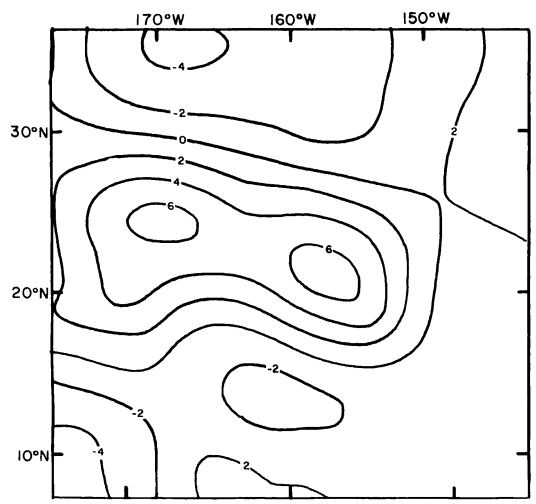

Fig. 4. The part of the observed geoid (in meters) that is coherent and phase with the topography.

Inversion of the Transfer Function

Equation (6) is still not in a form with a unique inverse. To put it in this form, a compensation model must be introduced. The first model tested was the local compensation model. For this case, (6) reduces to a Fredholm integral equation of the first kind:

$$Q_l = \frac{4\pi R^4}{M(2l+1)} \int_0^1 \mu^{l+2} \rho(\mu R)\, d\mu \tag{7}$$

Inversion of this equation corresponds to downward continuation, which is a highly unstable process. Errors in the transfer function show up as wild oscillations in the compensation model unless the function is constrained to be smooth.

A spectral expansion technique was used to find a best fitting local compensation model [*Parker*, 1977]. The observed

transfer function was converted from $Q(k)$ to Q_l so that a spherical geometry could be used for the inversion [*Dorman and Lewis*, 1970]. The compensation was constrained to be complete to a 7% uncertainty. Complete compensation is defined as

$$\rho_0 = -R \int_0^1 \rho(\mu R)\, d\mu \tag{8}$$

where ρ_0 is the density of the topography relative to water (1800 kg m^{-3}). The spectral expansion technique uses a weighted sum of eigenfunctions to represent $\rho(r)$. By varying the number of eigenfunctions a trade-off is made between resolution of the model and misfit of the transfer function. Four eigenfunctions were used. The two-norm misfit between the observed and model transfer function is $\chi^2 = 2.69$. The model transfer function is plotted as a dashed line in Figure 5. It fits within the uncertainties in the data with an average misfit of 0.34 standard deviations.

The compensation model with associated uncertainties is plotted on Figure 6. One thousand kilometers was chosen as the maximum compensation depth. Starting from the surface, 126% of the compensation occurs less than 70 km, −92% of the compensation is between 70 km and 300 km, and the remaining 68% of the compensation is below 300 km. A −92% compensation in the upper mantle may seem physically unsatisfactory, but it is easy to see why this feature is necessary. A positive compensating density centered about a depth z_0 causes the transfer function to be more positive at a wavelength of about $2\pi z_0$. Although the model has an acceptable fit to the data, we feel it should be rejected for two reasons. First, it is unlikely that these density contrasts could be maintained in the upper mantle for tens of millions of years. Second, positive compensating densities are not features of most compensation models, and there is no reasonable mechanism to explain them.

Since positive densities are physically undesirable, we proceed to see if there is a local compensation model, with only negative densities, that has an acceptable misfit. There are an infinite number of models within this class that could be tested. For this reason the model with the smallest misfit must be found. The misfit of this model is used to calculate the probability that the observed transfer function deviates from the model by this misfit or larger. If the probability of this occurrence is low, then the model can be rejected at some confidence level. Since this model is the model with the smallest misfit, every other model of this type can also be rejected. This method of rejecting classes of models was used by *Banks et al.* [1977].

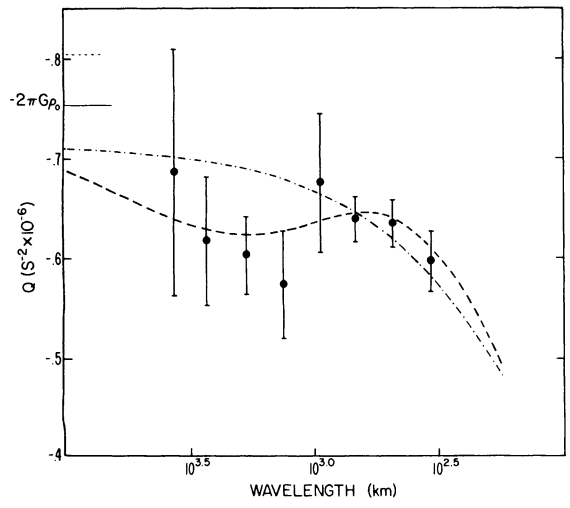

Fig. 5. Transfer function between Bouguer anomaly and topography. A density of 1800 kg m^{-3} was used to make the topographic correction. The dashed line is a model transfer function with positive and negative compensation; chain line is the best fitting model with only negative densities per unit topography.

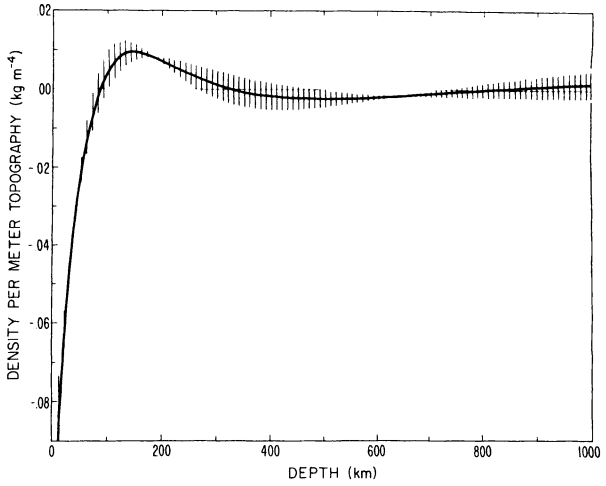

Fig. 6. Local compensation model represents the change in density per meter of topography. Uncertainties reflect the resolution of the model.

The best fitting, all negative model is most easily found by a linear programing algorithm. The details of solving the flat earth equivalent to (7) by a linear programing technique are described by *Banks and Swan* [1978]. For this inversion no constraint was placed upon the total amount of compensation. A maximum compensation depth of 1000 km was used. The best fitting model has all of its compensating density between the depths of 10 and 12.5 km. The compensation is 95% complete. The model transfer function is plotted as a chain line in Figure 5. The one-norm misfit is $\gamma_m = 7.23$. The fit to the data is good at the short wavelengths and is poor (more than one standard error) at wavelengths between 1000 and 2800 km.

From the misfit of the best fitting model the probability of exceeding this value with eight data is $P(\gamma > \gamma_m, 8) = 0.285$. The local compensation model with only negative densities can be rejected at the 72% confidence level.

Two classes of models were tested. The first was rejected because it requires an unphysical density structure in the upper mantle. The best fitting model from the second class is unacceptable because of its large misfit. *Banks et al.* [1977] reached this same conclusion when analyzing the transfer function for the continental United States. They interpreted this result as a need for a regional compensation mechanism. This model worked well for the continental U.S. data but is inappropriate for this case. For regional compensation, with positive density gradient, $\partial Q/\partial k$ is greater than zero for all wave numbers. Our data requires $\partial Q/\partial k$ to be less than zero over part of the wave number spectrum. What needs to be done is to reexamine the definition of local compensation to see if there is a more general class of models that can be tested.

Dorman and Lewis [1970] defined local compensation by stating that the compensating mass must lie directly beneath

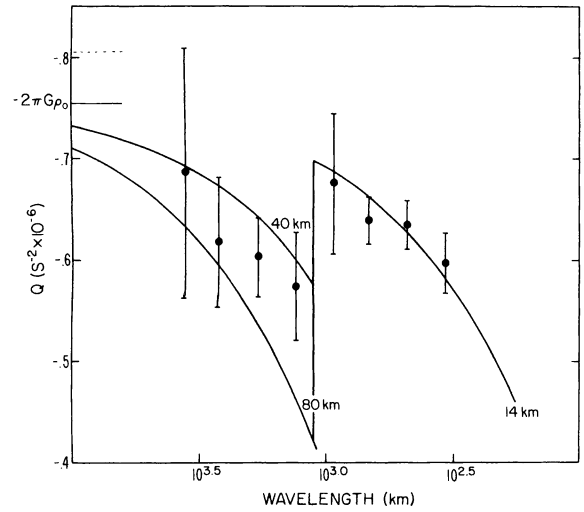

Fig. 7. Model transfer functions assuming linear, Airy-type compensation. Compensation depths are in kilometers. The vertical line corresponds to a wavelength of 1122 km.

the topographic load. Mathematically, they wrote

$$\Delta\rho(x', y', z') = \rho(z')t(x, y)\delta(x - x')\delta(y - y') \quad (9)$$

which relates the compensating density at the field point $\Delta\rho(x', y', z')$ to the topographic load $t(x, y)$ at the source point by a Green function of the form $\rho(z)\delta(x - x')\delta(y - y')$. Taking the fourier transform of (9) in the $\hat{x}$ and $\hat{y}$ directions, we find

$$\Delta P(\mathbf{k}, z) = \rho(z)T(\mathbf{k}) \quad (10)$$

where capitals denote the Fourier transform of the function (e.g. $\mathcal{F}_2[a(x, y, z)] = A(\mathbf{k}, z)$). The spherical equivalent of (10) was used to derive (7), and it encompasses both Pratt and Airy compensation models. The form of (9) implies that the local compensation mechanism is the same throughout the area. For the central Pacific this assumption is invalid. The data suggest that the shorter-wavelength topography is compensated at depths of 10–20 km, while the longer-wavelength loads are compensated much deeper. A way to fit the observed transfer function is to have one compensation mechanism $\rho_1(z)$ for wavelengths greater than 1100 km and another mechanism $\rho_2(z)$ for the shorter wavelengths. These ideas are represented by the following equation:

$$\Delta P(\mathbf{k}, z) = [\rho_1(z)H(k - k_0) + \rho_2(z)H(k_0 - k)]T(\mathbf{k}) \quad (11)$$

where $H(k)$ is the Heavyside step function and k_0 is some prescribed wave number. In the space domain, (11) represents a local compensation mechanism that is not constant throughout the region but varies horizontally, depending upon the spectral content of the topographic load.

This specific form of compensation was chosen because it allows acceptable fits to the data. Little or nothing is learned by determining the functions $\rho_1(z)$ and $\rho_2(z)$ with the best fitting transfer function. Figure 7 shows some examples of acceptable models. The solid lines are transfer functions for Airy compensation models with indicated compensation depths. For these models the compensation is complete. To calculate the longer-wavelength part of the transfer function, it is assumed that the lithosphere above the depth of compensation has a relative displacement equal to the long-wavelength topography. The density jump between the topographic density (2800 kg m^{-3}) and the lithospheric density (3300 kg m^{-3}) occurs at a depth of 14 km. Airy models with compensation depths between 40 and 80 km roughly bracket the uncertainties in the longer-wavelength data.

Discussion

We have found two negative density, local compensation models that fit the long- and short-wavelength parts of the observed transfer function. The data suggest that the division between the two should be placed at a wavelength of about 1100 km. For this model to be acceptable it must be shown that it is both physically reasonable and consistent with other geophysical observations. Since there is no mathematical model that will relate a mantle heat anomaly to both surface volcanism and swell formation, the physical reasonability of the proposed model cannot be clearly demonstrated. The best we can do is show that the model is not unreasonable. To do this, we present a very simple view of the tectonics in the area.

It is generally believed that the Hawaiian swell and the Hawaiian-Emperor seamount chain are the surface manifestations of the Pacific plate moving over a hot spot or mantle plume [*Wilson*, 1963]. By some poorly understood interaction between the plume and the moving plate a linear island chain is formed on the surface of the plate. The islands are composed of relatively young material and overlie a mature lithosphere. The compensation for the islands occurs at relatively shallow depths and is the result of volcanic loading [*Watts*, 1978]. For the swell the process is reversed. The broad swell in the topography is a result of its compensation. The two types of tectonic features are not separable in the space domain. Fortunately, partial separation is possible in the wave number domain. The separation is not complete because individual islands may contain a long-wavelength component. The observed transfer function has a rather abrupt jump at about 1100 km. This implies that either the swell dominates the amplitude spectrum for wavelengths greater than 1100 km or the long-wavelength part of individual islands has a deep compensation. There is no definite physical model that will explain a step in the observed transfer function, but a step is consistent with a very simplified picture of the tectonics in the central Pacific. It is also the most complex form of compensation that can be resolved by the data.

If the correct compensation model was chosen, then the results indicate that the deep compensating body contains very little power at wavelengths shorter than 1100 km. This sets a lower limit on the wavelengths of the heat source and/or pressure causing the swell.

If lithospheric reheating is the source of the swell compensation, then there is a simple way to estimate the strength and extent of the heat source from the topography. To derive this expression, a number of assumption must be made: (1) the lithosphere acts as a thermal boundary layer, (2) density anomalies result from thermal expansion, and (3) the lithosphere is isostatically supported. By requiring energy conservation and imposing these assumptions the following equation can be derived:

$$\frac{\partial d}{\partial t} + \mathbf{v} \cdot \nabla d = \frac{-\alpha}{C_p(\rho_m - \rho_w)}(q_\infty - q_s) \quad (12)$$

where d is the ocean depth, $\mathbf{v}$ is the velocity vector of the plate relative to the heat anomaly [*Minster and Jordan*, 1978], α is the coefficient of thermal expansion (3.5×10^{-5} °C^{-1}), C_p is the heat capacity (1050J kg^{-1} °C^{-1}), ρ_m is the lithospheric den-

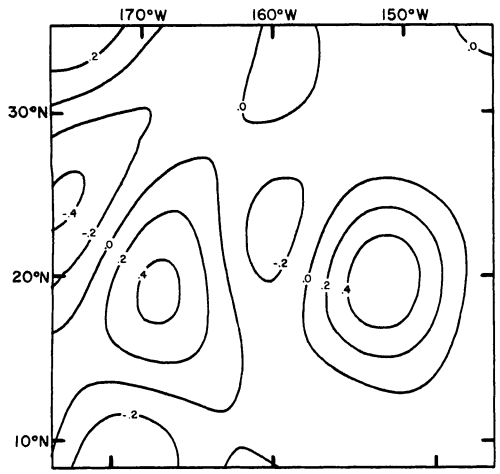

Fig. 8. Contour map of $q_\infty - q_s$ in watts per square meter.

sity (3300 kg m^{-3}), ρ_m is the density of seawater (1025 kg m^{-3}), q_∞ is the heat flow into the base of the lithosphere, and q_s is the surface heat flow. This equation was derived in a one-dimensional form by *Parsons and McKenzie* [1978]. If $\partial d/\partial t = 0$ and v is constant in time, then $q_\infty - q_s$ can be determined. From the transfer function analysis we found that the longer-wavelength ($\lambda > 1100$ km) topography was compensated by a deep mechanism. Using only this part of the topography in (12), an estimate is made of the amplitude and shape of the heat anomaly needed to uplift the Hawaiian swell.

Figure 8 shows a contour map of $q_\infty - q_s$. As expected, a nearly circular heat anomaly is needed to uplift the swell. There are many other features on the map that are unexpected and indicate a failure of this model. This model predicts that the longer-wavelength topography associated with the mid-Pacific mountains is currently being uplifted by a large heat anomaly. This is clearly incorrect. Many of the other longer-wavelength features away from the southeast end of the Hawaiian swell may have originated differently and at an earlier time than the swell. Since the time-dependent term was neglected in (12), the results are only valid for tectonic features with ages less than the time since the heat anomaly or velocity vector has changed significantly.

Detrick and Crough [1978] estimated that 40 times the normal surface heat flux is necessary to match the uplift rate at the S-E end of the swell. Using topographic wavelengths greater than 1100 km, we find a peak of 530 mW m^{-2} (13 heat flux units), and an average of 400 mW m^{-2} is needed. Using wavelength greater than 800 km, a peak of 550 mW m^{-2} is required. The width of the heat anomaly parallel to the velocity vector is about 1000 km, corresponding to a total heating time of 11 m.y. In writing (12) no heat transfer process was specified. *Crough* [1978] found that to fit the island subsidence data, the surface heat flux must rise from 45 mW m^{-2} to a peak of 70 mW m^{-2} over a time interval of 5 m.y. This implies that much of the heat needed to uplift the swell must be placed in the lithosphere at depths of about 40 km. Transferring the required amount of heat from the upper mantle to relatively shallow depths over an 11-m.y. period is a major problem with the lithospheric thinning hypothesis. We agree with *Detrick and Crough* [1978] that this mechanism cannot be conductive transport but must be some sort of rapid intrusion process.

As an alternative to the lithospheric reheating model, the Hawaiian swell could be supported by pressure exerted on the base of the lithosphere. This implies that a rising plume of material is supporting the swell. The compensation for this type of model is the low-density material in the rising plume at depths greater than 80 km. The mass deficiency in the plume is somewhat greater than the mass excess in the swell, since the low-density matrial must maintain both the flow pattern and the swell. For certain convection models the transfer function will look very similar to our observed transfer function [*McKenzie*, 1977].

By obtaining more longer-wavelength estimates of the transfer function we do not believe it will be possible to discriminate between the two models. The island subsidence data seem to indicate that the lithospheric thinning hypothesis is correct because it is difficult to conceive of a convection pattern that could support the islands along the Hawaiian-Emperor chain in the observed fashion.

CONCLUSIONS

Geoid heights and sea floor topography from the central Pacific were used to calculate a linear, isotropic transfer function in the wave number domain. A number of compensation models were tested to determine a class of acceptable models. A local compensation model with positive and negative compensating densities has a statistically good fit to the data. It was found to be unacceptable because it required a physically unreasonable density structure. The next model tested was constrained to have only negative compensating densities. The best fitting model is Airy compensation at a depth of 11 km. This model was also rejected because of a poor fit to the observed transfer function at wavelengths between 1000 and 3000 km. Since the Hawaiian swell has most of its power in this wavelength band, a local compensation model was proposed with compensation depending upon wave number. The shorter-wavelength data were insufficient to discriminate between local and regional compensation models. An Airy model with a 14-km depth of compensation fit within the uncertainties in the data. At the longer wavelengths, Airy compensation with depths between 40 and 80 km bracket the data. Some convection models [*McKenzie*, 1977] are consistent with the long-wavelength part of the observed transfer function. If the lithospheric thinning hypothesis is correct, then a heating anomaly with radius of about 600 km and a peak of 530 mW m^{-2} is required to fit the longer-wavelength ($\lambda > 1100$ km) topography.

Acknowledgements. We thank William Kaula and Leroy Dorman for their helpful suggestions and encouragement. Also the critical comments of the reviewers enabled us to make many beneficial changes in the original manuscript. This work was supported by NASA contract grant NGL 05-007-002 at the Department of Earth and Space Sciences, UCLA.

REFERENCES

Banks, R. J., and C. J. Swan, The isostatic compensation of east Africa, *Proc. Roy. Soc. London, 364*, 331–352, 1978.

Banks, R. J., R. L. Parker, and S. P. Huestis, Isostatic compensation on a continental scale: Local versus regional mechanisms, *Geophys. J. Roy. Astron. Soc., 51*, 431–452, 1977.

Brace, K. L., Preliminary ocean-area geoid from Geos-3 satellite radar altimetry, report, Def. Mapp. Agency, Aerosp. Center, St. Louis Air Force Station, Mo., 1977.

Chase, T. E., H. W. Menard, and J. Mammerickx, Bathymetry of the north Pacific, report, Inst. of Marine Resour., La Jolla, Calif., 1970.

Crough, S. T., Thermal origin of mid-plate hot-spot swells, *Geophys. J. Roy. Astron. Soc., 55*, 451–469, 1978.

Detrick, R. S., and S. T. Crough, Island subsidence, hot spots, and lithospheric thinning, *J. Geophys. Res., 83*, 1236–1244, 1978.

Dorman, L. M., and B. T. R. Lewis, Experimental isostasy, 1, Theory of the determination of the earth's isostatic response to a concentrated load, *J. Geophys. Res., 75*, 3357–3365, 1970.

Dorman, L. M., and B. T. R. Lewis, Experimental isostasy, 3, Inversion of the isostatic Green function and lateral density changes, *J. Geophys. Res., 77*, 3068–3077, 1972.

Ewing, J., M. Ewing, T. Actken, and W. J. Ludwig. North Pacific sediment layers measures by seismic profiling, in *The Crust and Upper Mantle of the Pacific Area, Geophys. Monogr. Ser.*, vol. 12, edited by L. Knopoff et al., AGU, Washington, D. C., 1968.

Lewis, B. T. R., and L. M. Dorman, Experimental isostacy, 2, An isostatic model for the U.S.A. derived from gravity and topographic data, *J. Geophys. Res., 75*, 3367–3386, 1970.

Matthews, C. J., Tables of the velocity of sound in pure water and sea water for use in echo-sounding and sound-ranging, *Rep. H.D. 282*, 52 pp., Hydrogr. Dep., Admiralty Office, London, 1939.

McDougall, I., Volcanic island chains and seafloor spreading, *Nature, 231*, 141–144, 1971.

McKenzie, D. P., Surface deformation, gravity anomalies and convection, *Geophys. J. Roy. Astron. Soc., 48*, 211–238, 1977.

McNutt, M. K., Continental and oceanic isostasy, Ph.D. thesis, 192 pp., Univ. of Calif., San Diego, 1978.

Menard, H. W., Depth anomalies and the bobbing motion of drifting islands, *J. Geophys. Res., 78*, 5128–5138, 1973.

Minster, J. B., and T. H. Jordan, Present-day plate motions, *J. Geophys. Res., 83*, 5331–5350, 1978.

Parker, R. L., Understanding inverse theory, A., *Rev. Earth Planet. Sci., 5*, 35–64, 1977.

Parsons, B., and D. P. McKenzie, Mantle convection and the thermal structure of the plates, *J. Geophys. Res., 83*, 4485–4495, 1978.

Shaw, H. R., Mantle convection and volcanic periodicity in the Pacific: Evidence from Hawaii, *Geol. Soc. Amer. Bull., 84*, 1505–1526, 1973.

Shaw, H. R., and E. D. Jackson, Linear island chains in the Pacific: Result of thermal plumes or gravitational anchors?, *J. Geophys. Res., 78*, 8634–8652, 1973.

Walcott, R. I., Flexure of the lithosphere at Hawaii, *Tectonophysics, 9*, 435–446, 1970.

Watts, A. B., Gravity and bathymetry in the central Pacific Ocean, *J. Geophys. Res., 81*, 1533–1553, 1976.

Watts, A. B., An analysis of isostasy in the world's oceans, 1, Hawaiian-Emperor seamount chain, *J. Geophys. Res., 83*, 5989–6003, 1978.

Wilson, J. T., Evidence from islands on the spreading of ocean flows, *Nature, 197*, 536–538, 1963.

(Received December 8, 1978;
revised September 17, 1979;
accepted January 14, 1980.)